

Lepton flavor violation and scalar dark matter in a radiative model of neutrino masses

Michael Klasen, David R. Lamprea

*Institut für Theoretische Physik,
Westfälische Wilhelms-Universität Münster,
Wilhelm-Klemm-Straße 9, D-48149 Münster, Germany*

Carlos E. Yaguna

*Max-Planck-Institut für Kernphysik,
Saupfercheckweg 1, 69117 Heidelberg, Germany*

Abstract

We consider a simple extension of the Standard Model that can account for the dark matter and explain the existence of neutrino masses. The model includes a vector-like doublet of $SU(2)$, a singlet fermion, and two scalar singlets, all of them odd under a new Z_2 symmetry. Neutrino masses are generated radiatively by one-loop processes involving the new fields, while the dark matter candidate is the lightest neutral particle among them. We focus specifically on the case where the dark matter particle is one of the scalars and its relic density is determined by its Yukawa interactions. The phenomenology of this setup, including neutrino masses, dark matter and lepton flavor violation, is analyzed in some detail. We find that the dark matter mass must be below 500 GeV to satisfy the relic density constraint. Lepton flavor violating processes are shown to provide the most promising way to test this scenario. Future $\mu \rightarrow 3e$ and μ - e conversion experiments, in particular, have the potential to probe the entire viable parameter space of this model.

1 Introduction

Neutrino masses and dark matter provide compelling evidence for physics beyond the Standard Model (SM). The gravitational effects of dark matter have been observed, for instance, in galaxies, clusters of galaxies, the large scale structure of the Universe, and in the cosmic microwave background radiation. Recently, the WMAP [1] and Planck [2] collaborations have determined the current dark matter density in the Universe to an unprecedented precision: $\Omega_{DM}h^2 = 0.1186 \pm 0.0031$. Oscillations experiments [3, 4, 5], on the other hand, have demonstrated that neutrinos have non-zero masses and have allowed us to measure the mixing and mass parameters in the neutrino sector [6].

Within the SM, neither neutrino masses nor dark matter can be explained, and current data does not tell us how the SM should be extended to account for

them. A particularly appealing possibility is that these two problems are not independent, as usually assumed, but arise from the same type of new physics. Moreover, this new physics may appear, as suggested by the WIMP paradigm of dark matter, at the TeV scale –the scale that is currently being probed by the LHC. In [7], many models of this type, featuring neutrino masses at one-loop, were found and classified. They all contain a small number of additional fields and a new discrete symmetry to stabilize the dark matter particle. In this paper, we study one of these models, denoted as T1-3 in [7].

In this model, which had been previously considered in [8, 9], the SM is extended with a vector-like SU(2) doublet, a singlet fermion, and two singlet scalars. We focus specifically on the case where the dark matter particle is a scalar and its relic density is determined by the Yukawa interactions (rather than the scalar ones), a possibility that to our knowledge has not been studied before. As we will show, in this setup strong correlations arise between dark matter, neutrino masses and lepton flavor violating (LFV) processes. In our analysis, we will investigate these correlations in some detail, partly relying on a scan over the parameter space of this model. First, we use a large sample of viable models to determine and study the regions that are consistent with the constraints from neutrino masses, $\mu \rightarrow e\gamma$, and dark matter. Then, we review the predictions for other LFV processes and the prospects for detection in future experiments. We find, in particular, that future searches for $\mu \rightarrow 3e$ and μ - e conversion in nuclei have the potential to probe the entire parameter space of this model. We also discuss alternative ways to test this scenario, including collider searches as well as direct and indirect dark matter searches.

The rest of the paper is organized as follows. In the next section we describe the model and introduce our notation. Then, in Sec. 3 we analyze semi-quantitatively the most relevant phenomenological aspects of this model, including neutrino masses, LFV processes, and dark matter. Our main results, based on a scan over the parameter space of this model, are presented in Sec. 4. First we examine the viable parameter space and then we demonstrate that the rates for several LFV processes are significant, offering the potential to probe this model thoroughly in the near future. In Sec. 5 we briefly discuss the possibility to test this scenario using collider or dark matter searches. Finally, we summarize and draw our conclusions in Sec. 6.

2 Description of the model

The model we consider belongs, in the generic classification of [10], to the T1-iii models of one-loop neutrino masses. It corresponds, in particular, to the model T1-3-A with $\alpha = 0$ (where α is related to the hypercharge), as defined in [7]. In this model the SM particle content is extended with a vector-like fermion (or two chiral fermion) doublet under SU(2), D, D' , one left-handed singlet fermion, S , and two real scalar singlets ϕ_i ($i = 1, 2$). To guarantee the stability of the dark matter candidate and to prevent tree-level neutrino masses, the SM gauge group is extended with a Z_2 discrete symmetry, under which all the new fields are odd, while the SM fields are even. Thus, the charges of the new particles under the SU(2) \otimes U(1) \otimes Z_2 symmetry are given by

$$D = \begin{pmatrix} \psi \\ E \end{pmatrix} \sim (2, -\frac{1}{2}, -), \quad D' = \begin{pmatrix} -E' \\ \psi' \end{pmatrix} \sim (2, \frac{1}{2}, -), \quad (1)$$

for the fermion doublets and

$$S \sim (1, 0, -), \quad \phi_i \sim (1, 0, -) \quad (2)$$

for the fermion and scalar singlets, respectively. The SM electroweak sector under the same symmetry transforms instead as

$$H = \begin{pmatrix} \phi^+ \\ \phi^- \end{pmatrix} \rightsquigarrow \begin{pmatrix} 0 \\ \frac{1}{\sqrt{2}}(v+h) \end{pmatrix} \sim (2, \frac{1}{2}, +), \quad L_i = \begin{pmatrix} \nu_{iL} \\ e_{iL} \end{pmatrix} \sim (2, -\frac{1}{2}, +), \quad (3)$$

for the doublets ($i = 1\dots 3$) and

$$e_{iR} \sim (1, 1, +) \quad (4)$$

for the SU(2) singlets. The most general Lagrangian consistent with the symmetry and the particle content of our model can be written as

$$\mathcal{L} = \mathcal{L}_{SM} - V(H, \phi_i) - \alpha_{ij} \overline{D'} L_j^c \phi_i - \mu \overline{D^c} D' - \beta_1 \overline{D^c} H S - \beta_2 \overline{D'} \tilde{H} S^c - \frac{1}{2} m_S \overline{S^c} S + \text{h.c.}, \quad (5)$$

where \mathcal{L}_{SM} is the SM Lagrangian, $V(H, \phi_i)$ is the scalar potential, and $\tilde{H} = i\sigma_2 H^*$. This Lagrangian includes a Dirac mass term for the vector-like doublet fermion, a Majorana mass term for the singlet fermion, Yukawa terms between the new singlet and doublet fermions, and a new Yukawa interaction for the SM lepton doublets.

It is precisely this new interaction that allows to obtain non-zero neutrino masses. At tree-level, neutrinos remain massless because the scalar fields ϕ_i do not acquire a vev – the Z_2 symmetry must remain exact to explain the dark matter. It is only at one-loop that neutrinos will get a Majorana mass. In fact, it is not difficult to verify that this Lagrangian generically violates lepton number. Being real scalar fields, ϕ_i should have zero lepton number and likewise the singlet Majorana fermion S . But then the terms with coefficients α_{ij} , β_1 and β_2 cannot simultaneously conserve lepton number. Lepton number would still be a good symmetry in the limits $\alpha_{ij} = 0$ or $\beta_1 = \beta_2 = 0$. Neutrino masses, which are lepton-number violating, must therefore vanish in such cases.

Once expanded, the Lagrangian includes the following mass terms

$$\mathcal{L}_m = -\mu \overline{\psi^c} \psi' - \mu \overline{E^c} E' - \frac{v\beta_1}{\sqrt{2}} \overline{\psi^c} S - \frac{v\beta_2}{\sqrt{2}} \overline{\psi'} S^c - \frac{1}{2} m_S \overline{S^c} S - \frac{1}{2} m_{\phi_i} \phi_i^2 + \text{h.c.} \quad (6)$$

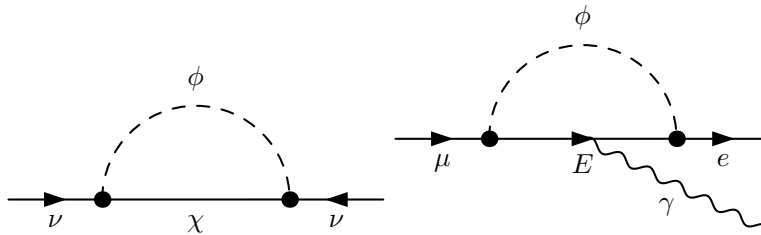


Figure 1: Left: The diagram responsible for neutrino mass generation. Right: One of the diagrams contributing to $\mu \rightarrow e\gamma$.

and the following couplings with the SM particles

$$\mathcal{L}_Y = \alpha_{ij} \bar{\psi}' \nu_{jL}^c \phi_i + \alpha_{ij} \bar{E}' e_{jL}^c \phi_i + \frac{\beta_1}{\sqrt{2}} \bar{\psi}^c S h + \frac{\beta_2}{\sqrt{2}} \bar{\psi}' S^c h + \text{h.c.} \quad (7)$$

Defining $\Psi := (\psi, \psi', S)$, the Majorana mass matrix for the odd neutral fermions can be written, from Eq. (6), as

$$m_\Psi = \begin{pmatrix} 0 & \mu & \frac{v\beta_1}{\sqrt{2}} \\ \mu & 0 & \frac{v\beta_2}{\sqrt{2}} \\ \frac{v\beta_1}{\sqrt{2}} & \frac{v\beta_2}{\sqrt{2}} & m_S \end{pmatrix}. \quad (8)$$

This matrix can be diagonalized via the transformation

$$\Psi_i \equiv \xi_{ij} \chi_j, \quad (9)$$

where ξ is the mixing matrix and χ_i are the physical mass eigenstates with masses m_i such that $m_i < m_j$ for $i < j$.

In addition to these three Majorana fermions, the spectrum contains also a charged Dirac fermion with mass $\mu \equiv m_E$ – see Eq. (6) – constrained by collider searches [11] to be larger than about 103.5 GeV, and two neutral scalars with masses $m_{\phi_{1,2}}$.

3 Phenomenology

In this section, the main phenomenological features of this model are discussed, in particular regarding neutrino masses, dark matter, and lepton flavor violating processes.

3.1 Neutrino masses

Radiative mechanisms are a very attractive way of explaining neutrino masses and have been implemented within many different scenarios – see e.g. [12, 13, 14, 15, 16, 17, 18, 19, 20, 21, 9, 22]. In the model we consider, neutrino masses are obtained through a radiative mechanism at one-loop. The relevant diagram, shown in the left panel of Fig. 1, contains the neutral odd particles (scalars and fermions) running in the loop. Since one of these neutral particles will be the dark matter candidate, some connection between dark matter and neutrino

masses is necessarily present. The evaluation of the diagram yields, for a given neutral fermion (k) and a given singlet scalar (r), the following contribution to the neutrino mass matrix

$$M_{ij}^{k,r} = \frac{1}{16\pi^2} \Gamma_{jk}^r \Gamma_{ik}^r m_k \times \left((1 + \Delta) - \frac{m_k^2}{m_k^2 - m_r^2} \log \left(\frac{m_k^2}{\mu_R^2} \right) + \frac{m_r^2}{m_k^2 - m_r^2} \log \left(\frac{m_r^2}{\mu_R^2} \right) \right), \quad (10)$$

where $\Gamma_{lm}^r = \alpha_{rl} \xi_{2m}$ is the coupling between ϕ_r , χ_m , and ν_L^c . In this equation, $\Delta \propto \frac{1}{\epsilon}$ ($\epsilon = 4 - d$) whereas μ_R is an arbitrary renormalization constant. The neutrino mass matrix element m_{ij}^ν can therefore be computed as a sum over all the fermions and scalars that run in the loop:

$$m_{ij}^\nu = \sum_{k,r} M_{ij}^{k,r} = \sum_{k,r} \frac{1}{16\pi^2} m_k \alpha_{ri} \alpha_{rj} \xi_{2k} \xi_{2k} \left(\frac{m_k^2}{m_k^2 - m_r^2} \log \left(\frac{m_k^2}{m_r^2} \right) \right), \quad (11)$$

where we have used the fact that

$$\sum_k \xi_{2k} m_k \xi_{k2}^T = (m_\Psi^T)_{22} = 0. \quad (12)$$

Notice that, as expected, the final result is finite and thus independent of the unphysical renormalization factor μ_R . As anticipated, the neutrino mass matrix vanishes in the limit $\alpha_{ij} = 0$, where lepton number is conserved. To see that it also vanishes in the limit $\beta_1 = \beta_2 = 0$, we can diagonalize Eq. (8) analytically at leading order in $\beta_1, \beta_2 \ll 1$ to obtain

$$\xi = \begin{pmatrix} \frac{i}{\sqrt{2}} & \frac{1}{\sqrt{2}} & \frac{2m_S \beta_1 + 4\mu \beta_2}{m_S^2 - 4\mu^2} v \\ -\frac{i}{\sqrt{2}} & \frac{1}{\sqrt{2}} & \frac{2m_S \beta_2 + 4\mu \beta_1}{m_S^2 - 4\mu^2} v \\ i \frac{\beta_2 - \beta_1}{m_S + 2\mu} \frac{v}{\sqrt{2}} & \frac{\beta_1 + \beta_2}{2\mu - m_S} \frac{v}{\sqrt{2}} & 1 \end{pmatrix} + \mathcal{O}(\beta_1^2, \beta_2^2, \beta_1 \beta_2). \quad (13)$$

Hence, the neutrino masses in Eq. (11) can be expressed as

$$m_{ij}^\nu = \sum_r \frac{1}{16\pi^2} m_S \alpha_{ri} \alpha_{rj} \left(\frac{2m_S \beta_2 + 4\mu \beta_1}{m_S^2 - 4\mu^2} \right)^2 v^2 \left(\frac{m_S^2}{m_S^2 - m_r^2} \log \left(\frac{m_S^2}{m_r^2} \right) \right), \quad (14)$$

which indeed goes to zero in the limit $\beta_{1,2} \rightarrow 0$. Since the experimentally determined neutrino masses are tiny, either α_{ij} or $\beta_{1,2}$ must be suppressed. To estimate the typical values of the parameters that give rise to neutrino masses consistent with the data, we can evaluate Eq. (14) for masses around the TeV scale to obtain

$$m^\nu \sim 0.1 \text{ eV} \times \left(\frac{m_S}{1 \text{ TeV}} \right) \left(\frac{\alpha_{ij} \beta_{1,2}}{10^{-5}} \right)^2. \quad (15)$$

Notice that neutrino masses cannot distinguish whether it is the α_{ij} or the $\beta_{1,2}$ that are suppressed but, as we will see later, the dark matter constraint only allows the latter option.

Since α_{ij} and $\beta_{1,2}$ enter both quadratically in m^ν , the required coupling suppression is not as large as in the well-known scotogenic model [16], where

λ_5 can be of order 10^{-10} [23]. In our model the coupling suppression is only of order 10^{-5} .

It is easy to verify that, in our scenario, the neutrino mass matrix has only two non-zero eigenvalues. This result is a direct consequence of the two real scalar fields that interact with the lepton doublets. To obtain three non-zero neutrino masses, one more scalar field would be needed. But, since current neutrino data is consistent with one massless neutrino, we will stick to this minimal framework, as outlined in the previous section. The neutrino spectrum, therefore, is necessarily hierarchical and we assume it henceforth to be of normal type (NH).

The resulting neutrino mass matrix, Eq. (11), can be written in a way reminiscent of the seesaw mechanism as

$$m_{ij}^\nu = \alpha_{ir}^\top F_r \alpha_{rj}, \quad (16)$$

with

$$F_r = \sum_k \frac{1}{16\pi^2} m_k \xi_{2k} \xi_{2k} \left(\frac{m_k^2}{m_k^2 - m_r^2} \log \left(\frac{m_k^2}{m_r^2} \right) \right). \quad (17)$$

This form of the neutrino mass matrix allows us to use a slightly modified version of the Casas-Ibarra parametrization [24]. Explicitly, we have that

$$\alpha = iU^* \sqrt{m^\nu} R \sqrt{F^{-1}}, \quad (18)$$

where $m^\nu = \text{diag}(0, m_2^\nu, m_3^\nu)$ are the light neutrino masses, U is the PMNS neutrino mixing matrix, $F = \text{diag}(F_1, F_2)$, and R is a 3×2 matrix such that $RR^T = 1$. This matrix depends on a single parameter, θ , as [25]

$$R = \begin{pmatrix} 0 & 0 \\ \cos \theta & \pm \sin \theta \\ -\sin \theta & \pm \cos \theta \end{pmatrix}. \quad (19)$$

Equation (18) provides, for a given set of scalar and fermion mass parameters, the most general form of the α_{ij} couplings that is consistent with the observed neutrino data, which are used as input parameters. In other words, the constraints on neutrino masses and mixing angles are automatically incorporated into the structure of α as given by Eq. (18), simplifying enormously the analysis of the viable parameter space.

3.2 Lepton flavor violating processes

The existence of non-zero neutrino masses and mixing angles also imply the violation of the lepton flavor. In consequence, processes involving the charged leptons and where the lepton flavor is not conserved – lepton flavor violating (LFV) processes – such as $\mu \rightarrow e\gamma$ and $\mu \rightarrow 3e$ should occur at some level in this model. The relevant diagrams appear first at one-loop, as illustrated in the right panel of Fig. 1 for $\mu \rightarrow e\gamma$. Notice that the fermion running in the loop is now the Dirac charged fermion rather than the neutral ones.

In this model, the $\mu \rightarrow e\gamma$ branching ratio can be evaluated to be

$$\text{BR}(\mu \rightarrow e\gamma) = \frac{3\alpha_{\text{em}}}{64\pi G_{\text{F}}^2 m_E^4} \left| \sum_r \alpha_{r,1} \alpha_{r,2} G(m_{\phi_r}^2/m_E^2) \right|^2, \quad (20)$$

LFV Process	Present Bound	Future Sensitivity
$\mu \rightarrow e\gamma$	5.7×10^{-13} [27]	6×10^{-14} [28]
$\tau \rightarrow e\gamma$	3.3×10^{-8} [29]	$\sim 3 \times 10^{-9}$ [30]
$\tau \rightarrow \mu\gamma$	4.4×10^{-8} [29]	$\sim 3 \times 10^{-9}$ [30]
$\mu \rightarrow eee$	1.0×10^{-12} [31]	$\sim 10^{-16}$ [32]
$\tau \rightarrow \mu\mu\mu$	2.1×10^{-8} [33]	$\sim 10^{-9}$ [30]
$\tau^- \rightarrow e^- \mu^+ \mu^-$	2.7×10^{-8} [33]	$\sim 10^{-9}$ [30]
$\tau^- \rightarrow \mu^- e^+ e^-$	1.8×10^{-8} [33]	$\sim 10^{-9}$ [30]
$\tau \rightarrow eee$	2.7×10^{-8} [33]	$\sim 10^{-9}$ [30]
$\mu^-, \text{Ti} \rightarrow e^-, \text{Ti}$	4.3×10^{-12} [34]	$\sim 10^{-18}$ [35, 36]
$\mu^-, \text{Au} \rightarrow e^-, \text{Au}$	7×10^{-13} [37]	
$\mu^-, \text{Al} \rightarrow e^-, \text{Al}$		$10^{-15} - 10^{-18}$ [38]
$\mu^-, \text{SiC} \rightarrow e^-, \text{SiC}$		10^{-14} [39]

Table 1: Current experimental bounds and future sensitivities for the most important LFV observables.

where

$$G(x) = \frac{2 - 3x - 6x^2 + x^3 + 6x \log x}{6(1-x)^4}. \quad (21)$$

An analogous expression holds for the related processes $\tau \rightarrow \mu\gamma$ and $\tau \rightarrow e\gamma$. For other processes, the analytical expressions are more complicated and are therefore better studied numerically (with the help of FlavorKit [26]), as we will do in the next section.

Typically, $\mu \rightarrow e\gamma$ provides the most stringent constraint among LFV processes, so many works have focused on this process. But, as emphasized in [23] this situation might drastically change in the near future thanks to the significant improvements that will likely be achieved for other LFV processes, as shown in Tab. 1. Particularly relevant will be the expected limits on $\mu \rightarrow 3e$ and μ - e conversion in nuclei, which may improve, respectively, by up to four and six orders of magnitude [40]. It is important, therefore, not to limit the discussion on LFV processes to $\mu \rightarrow e\gamma$ but to consider also these other promising processes when analyzing future detection prospects.

A crucial difference between neutrino masses and LFV processes, both of which appear at one-loop in this model, is that the former violate lepton number, while the latter do not. As a result, LFV processes depend only on the α_{ij} couplings but not on $\beta_{1,2}$ or m_S , as shown explicitly above for $\mu \rightarrow e\gamma$.

To obtain observable rates for LFV processes, two conditions must generically be satisfied: the particles in the loop must not be that heavy and the relevant couplings, α_{ij} in this case, should be of order 1-0.1. As we saw in the previous subsection, this second requirement is compatible with neutrino masses as long as the beta parameters are tiny, $\beta_{1,2} \ll 1$. Next, we show that, under certain circumstances, these requirements are actually enforced by the dark matter constraint.

3.3 Dark matter phenomenology

The dark matter candidate in this model is the lightest neutral odd (under the Z_2) particle in the spectrum, which can be one of the three fermions, or one of

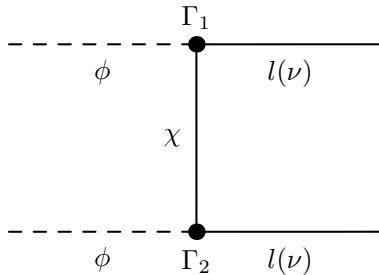


Figure 2: General diagram contributing to the relic density computation.

the two scalars. Since the fermion and scalar masses are free parameters, both of these possibilities can be realized in this model. When the dark matter is a fermion, the resulting phenomenology is very similar to that of the so-called singlet-doublet fermion model [41, 42, 43], which has been extensively studied in the recent literature – see e.g. [44, 45, 46, 47, 48]. It has been shown, in particular, that by adjusting the mixing between the singlet and the doublet one can obtain the correct relic density, via freeze-out in the early Universe, for dark matter masses below 1 TeV or so. The additional scalars present in this model may slightly modify this picture due to coannihilation effects, as recently demonstrated in [9].

When the dark matter is the scalar, two different scenarios can be distinguished depending on its dominant interactions. Scalars, in fact, not only have the Yukawa interactions explicitly shown in Eq. (7) but also scalar interactions with the SM Higgs boson, implicitly included in $V(H, \phi_i)$. These scalar interactions give rise to the so-called singlet scalar or Higgs-portal model [49, 50, 51], where dark matter annihilations are mediated by the Higgs boson. These models are quite predictive and have been the subject of many previous analyses [52, 53, 54, 55, 56, 57, 58, 59, 60, 61]. In this paper we assume instead that the scalar dark matter interacts dominantly via the Yukawa interactions in Eq. 7. Thus, it will annihilate into leptons via t -channel fermion-mediated diagrams with a cross section proportional to α_{ij}^4 – see Fig. 2. Consequently, non-trivial correlations between neutrino masses, LFV processes and dark matter are expected. In fact, we can already state that to obtain a relic density in agreement with the observations, α_{ij} should be of order one and the mediators cannot be that heavy, which are essentially the same conditions that ensure observable rates for LFV processes, as we saw in the previous subsection. Throughout the rest of the paper, we will be working on this specific framework where the dark matter particle is a scalar, denoted by ϕ_1 , that interacts dominantly via the Yukawa terms with the SM lepton doublets. Notice that as a result, the dark matter turns out to be *leptophilic*, with important implications for the direct detection prospects, as will be discussed in Sec. 5.

In this setup, dark matter annihilates into charged leptons with a cross section given, in the non-relativistic limit, by [62]

$$\sigma v(\phi_1 \phi_1 \rightarrow \ell^+ \ell^-) = \frac{\alpha_{1\ell}^4 v^4}{60\pi} \frac{m_{\phi_1}^2}{m_{\phi_1}^4 + m_E^4}. \quad (22)$$

This cross section gets suppressed as the dark matter mass or the charged

fermion mass increases. Notice also that it has a strong velocity dependence ($\propto v^4$). During freeze-out, this velocity suppression is not that important but today, when $v \sim 10^{-3}$ in our Galaxy, it pretty much prevents the annihilation of dark matter particles into two charged leptons, significantly affecting the dark matter indirect detection signatures in this model.

The annihilation into neutrinos proceeds through a similar diagram, but it turns out to be negligible due to the fact that the exchanged fermion is a Majorana rather than a Dirac particle. Thus, only charged leptons contribute to the total annihilation rate. In our numerical analysis we will see that, due to the constraints from $\mu \rightarrow e\gamma$, it is the $\tau^+\tau^-$ final state that actually dominates the cross section.

To obtain an accurate prediction of the dark matter relic density, we implemented this model into DarkSUSY [63] (micrOmegas [64] gives numerical errors in the evaluation of the annihilation cross section). Specifically, we use the σv above to compute the invariant annihilation rate as defined in the DarkSUSY manual, and use the function `dsrdens()` to obtain the relic density. We also verified that the computations done in this way match the approximate analytical results known in the literature.

4 Numerical results

In this model non-trivial correlations between dark matter, neutrino masses and lepton flavor violating processes are expected. The reason is that, on the one hand, the dark matter constraint requires sizable α_{ij} couplings between the dark matter and the SM leptons. On the other hand, these couplings cannot be flavor diagonal because they determine the structure of the neutrino mass matrix. Consequently, these couplings induce significant rates for LFV processes. In this section, we use a scan over the parameter space of this model to numerically study these correlations. To that end, we first obtain a large sample of viable models that we use to analyze the regions in the parameter space of the model that are consistent with current bounds. Then, we analyze the prediction for LFV processes and demonstrate that future LFV experiments have the potential to probe most of the viable models.

4.1 The viable parameter space

The relevant free parameters of this model are just seven: $m_{\phi_{1,2}}$, μ , m_S , $\beta_{1,2}$ and θ . Our sample of viable models is obtained after scanning over the allowed range of these parameters and imposing the following constraints: the dark matter relic density ($\Omega_{DM}h^2 \sim 0.12$), the $\mu \rightarrow e\gamma$ upper limit – $\text{BR}(\mu \rightarrow e\gamma) < 5.7 \times 10^{-13}$ –, and perturbativity (somewhat arbitrarily, we require all dimensionless couplings to be smaller than three). Regarding the dark matter relic density, we assume that it is obtained via thermal freeze-out in the early Universe and that coannihilation effects play no role in its determination, as is generically the case. To enforce this latter condition, we require all other masses to be larger than $1.2m_{\phi_1}$. The upper bound on the mass parameters is taken to be 10 TeV. By construction, all our models are consistent with neutrino data, for we use as input the experimental data on neutrino masses and mixing angles

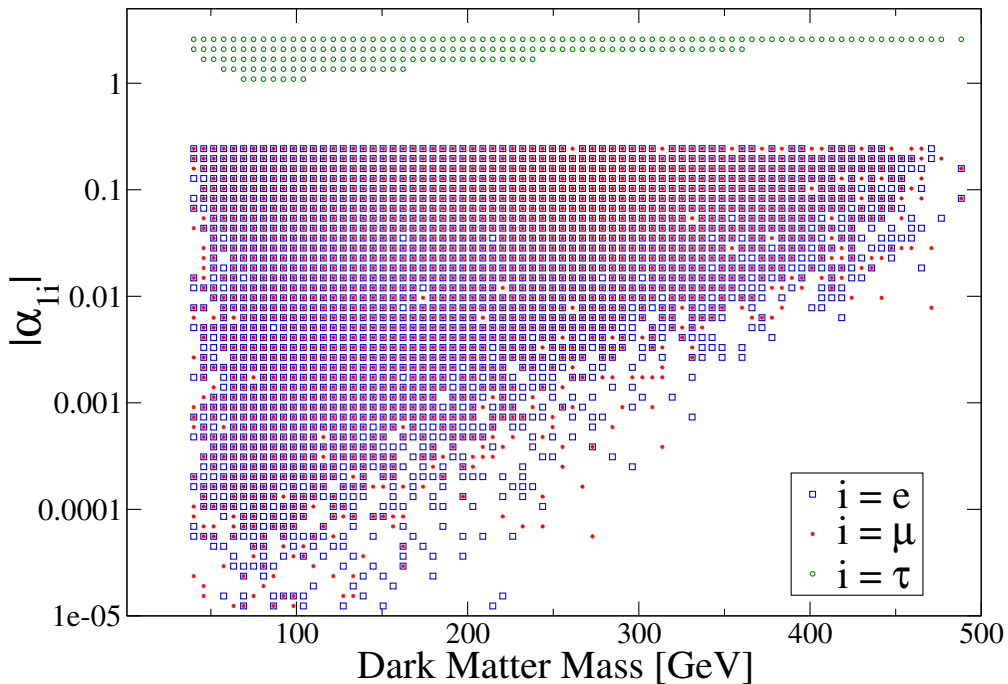


Figure 3: The viable models projected onto the plane (m_ϕ, α_{i1}) . The α_{i1} couplings determine the dark matter annihilation rate and must therefore be non-negligible.

according to Eq. (18). In our analysis, we made use of SARAH and the BSM Tool Box scripts [65], which facilitate the whole process.

Let us begin by examining the viable regions of the parameter space. Figure 3 displays our set of viable models in the plane (m_ϕ, α_{i1}) , with $i = e, \mu, \tau$. Notice that, as a result of the strong bounds from $\mu \rightarrow e\gamma$, $\alpha_{\tau 1} \gg \alpha_{e1}, \alpha_{\mu 1}$. Thus, dark matter annihilates dominantly into the $\tau^+\tau^-$ final state. In fact, $\alpha_{\tau 1}$ increases with the dark matter mass, going from about one for $m_\phi \sim 50$ GeV to three – the perturbativity limit we imposed – for $m_\phi \sim 500$ GeV. Consequently, the dark matter particle in this scenario must be light, lying below 500 GeV.

The condition $\alpha_{1\tau} \gg \alpha_{1e}, \alpha_{1\mu}$ is not satisfied for generic values of the α_{ij} couplings. According to Eq. (18), we have that

$$\frac{\alpha_{1\tau}}{\alpha_{1e}} = \frac{\sqrt{m_2^{\nu}} \cos(\theta)(-c_{23}s_{12}s_{13} - c_{12}s_{23}) - \sqrt{m_3^{\nu}} \sin(\theta)c_{13}c_{23}}{\sqrt{m_2^{\nu}} \cos(\theta)c_{13}s_{12} - \sqrt{m_3^{\nu}} \sin(\theta)s_{13}}, \quad (23)$$

and

$$\frac{\alpha_{1\tau}}{\alpha_{1\mu}} = \frac{\sqrt{m_2^{\nu}} \cos(\theta)(-c_{23}s_{12}s_{13} - c_{12}s_{23}) - \sqrt{m_3^{\nu}} \sin(\theta)c_{13}c_{23}}{\sqrt{m_2^{\nu}}(c_{12}c_{23} - s_{12}s_{13}s_{23}) \cos(\theta) - c_{13}\sqrt{m_3^{\nu}}s_{23} \sin(\theta)}. \quad (24)$$

If we now require $\alpha_{1\tau} \gg \alpha_{1e}, \alpha_{1\mu}$ we get that, for typical values of the neutrino parameters, $\theta \sim 0.35$. The left panel of Fig. 4 shows the value of θ for our set of viable models. We see that, indeed, θ varies only within a narrow range around

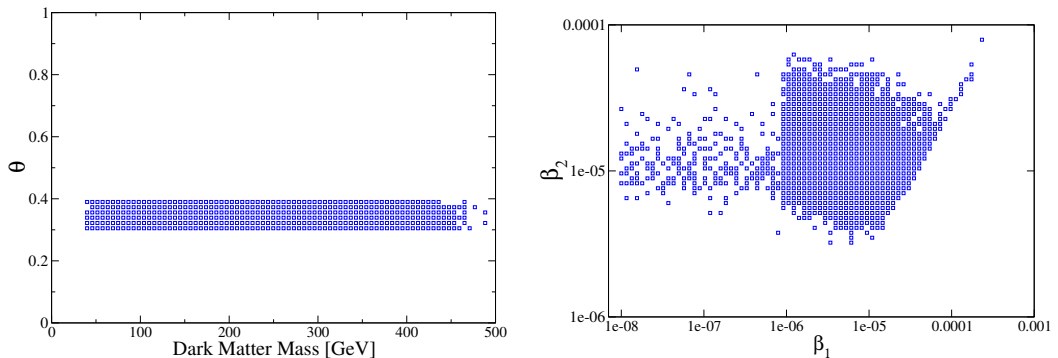


Figure 4: Left: The viable models projected onto the plane (m_ϕ, θ) . Notice that the experimental constraints essentially select a single value of θ . Right: The viable models projected onto the plane (β_1, β_2) . Neutrino masses require $\beta_{1,2}$ to be small.

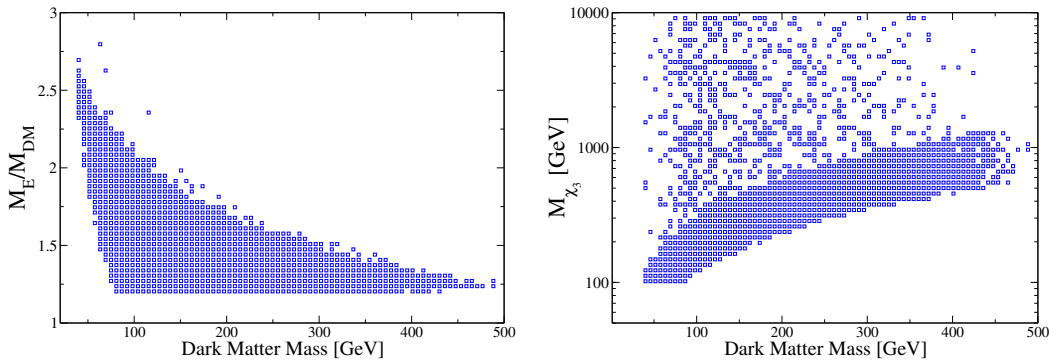


Figure 5: Left: The viable models projected onto the plane (m_ϕ, m_{χ_1}) . The relic density constraint favors a χ_1 not much heavier than the dark matter (ϕ). Right: The viable models projected onto the plane (m_ϕ, m_{χ_3}) . Notice that the heaviest odd fermion, χ_3 , rarely has a mass above 1 TeV.

0.35. Thus, the dark matter constraint and the limits on LFV processes select a rather specific value for θ .

As we saw in the previous section, the parameters β_1 and β_2 must be tiny so that neutrino masses are sufficiently suppressed. The right panel of Fig. 4 displays the viable models in the plane (β_1, β_2) and confirms that this is really the case. These parameters are never larger than about 10^{-4} . β_1 could be much smaller than that, whereas β_2 varies only between 10^{-4} and about 10^{-6} . Notice that the dark matter constraint plays also a role in this case, as it enforces a sizable value of the α_{ij} couplings.

The relic density depends strongly on the masses of the dark matter particle and of the Dirac fermion that mediates the annihilation processes. The left panel of Fig. 5 displays the ratio m_E/m_{ϕ_1} as a function of the dark matter mass for our sample of viable points. The lower limit on m_E/m_{ϕ_1} is 1.2 (to prevent coannihilations) and we see from the figure that it tends to that value at the

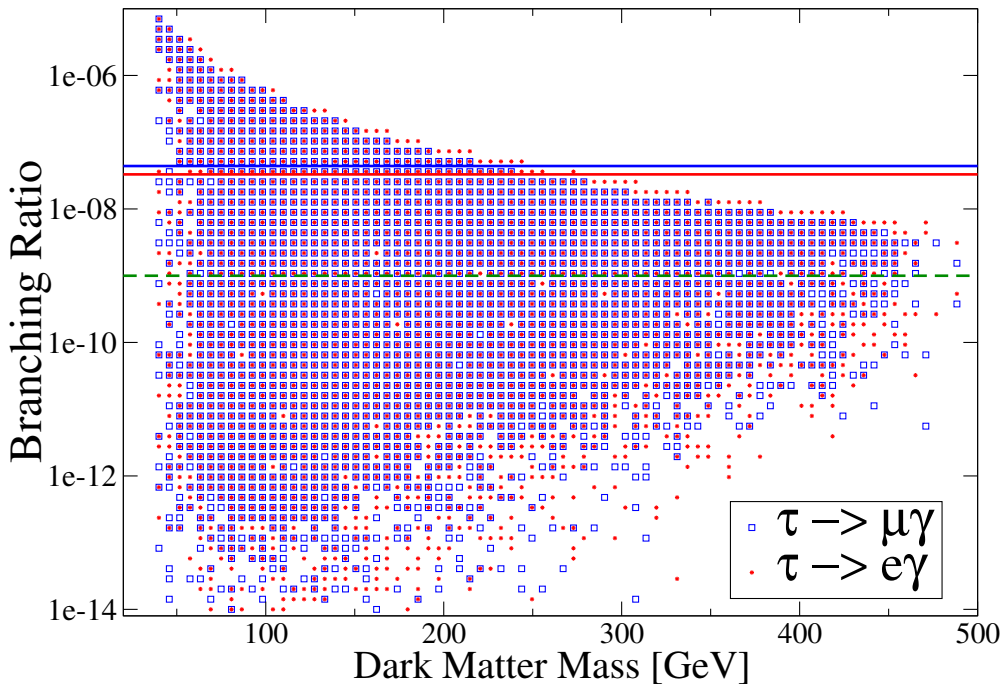


Figure 6: The branching ratios $\tau \rightarrow \mu\gamma$ (blue squares) and $\tau \rightarrow e\gamma$ (red stars) as a function of the dark matter mass for our sample of viable models. The solid lines show the current bound for each process while the dashed line corresponds to the expected future sensitivity.

highest dark matter masses. In any case, m_E is never much larger than the dark matter mass. The dark matter constraint thus requires the existence of a charged fermion with a mass below 600 GeV.

Two of the three neutral fermions have a mass very close to $m_E \sim \mu$ as a result of the small mixing induced by the parameters $\beta_{1,2} \ll 1$ (the mixing among the neutral fermions is very small). The other neutral fermion, with mass $\sim m_S$, can have a much larger mass. The right panel of Fig. 5 displays the dark matter mass versus the mass of the heaviest neutral fermion, M_{χ_3} . Even though this mass can reach its upper limit (10 TeV), in most models it tends to be close to the dark matter mass. The spectrum in this setup is thus rather compressed.

4.2 Implications for LFV processes

In this section we study in detail the predicted rates for the most relevant LFV processes and compare them against current limits and expected sensitivities in planned experiments. As we will see, this scenario predicts sizable rates for several LFV processes, particularly $\mu \rightarrow 3e$ and $\text{CR}(\mu - e)$. These processes, in fact, provide the most promising way of probing this model in the near future.

Let us begin our analysis with LFV τ decays. Figure 6 displays the branching ratios for the decay processes $\tau \rightarrow \mu\gamma$ (blue squares) and $\tau \rightarrow e\gamma$ (red stars) as a function of the dark matter mass. Both processes feature the same behaviour

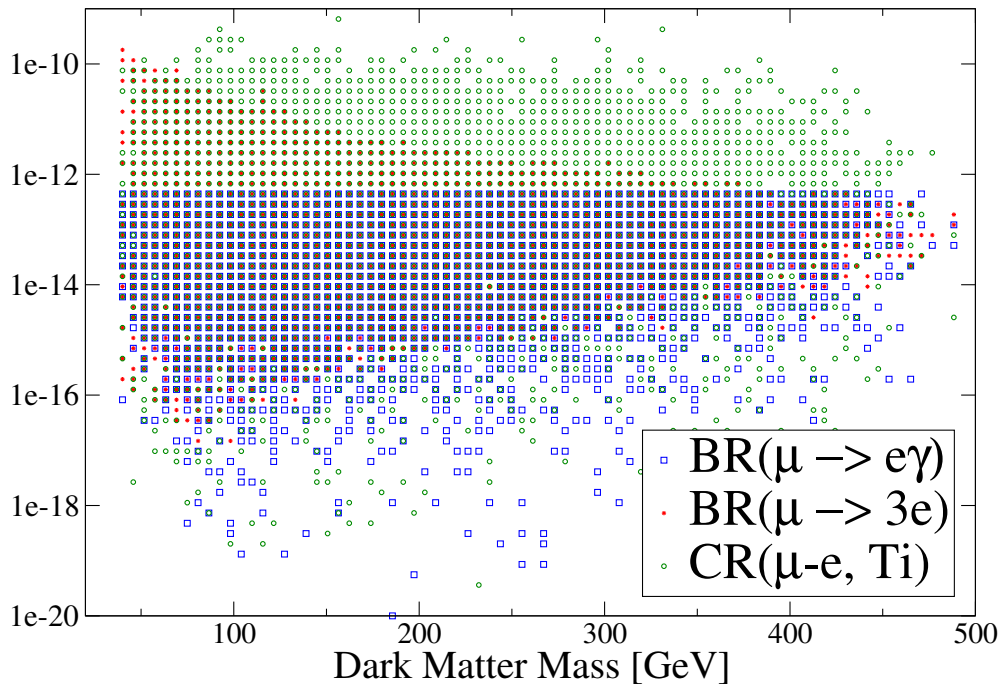


Figure 7: The rates of the most relevant μ - e LFV processes as a function of the dark matter mass for our sample of viable models.

– its maximum value decreasing with the dark matter mass – and similar values at a given mass. These branching ratios vary over a wide range at low masses (from 10^{-5} to 10^{-13} or so) but tend to concentrate between 10^{-8} and 10^{-10} at higher dark matter masses. For comparison, current limits are also shown in the figure as solid lines, as well as the expected future sensitivity for both processes (dashed line). Interestingly, we see that current limits can be violated for dark matter masses below 250 GeV or so. In addition, future experiments will be able to probe a significant fraction of models over the entire range of dark matter masses.

Let us now switch to μ - e LFV processes, which are typically more relevant. Figure 7 shows, as a function of the dark matter mass, the $\mu \rightarrow e\gamma$ (blue squares) and $\mu \rightarrow 3e$ (red stars) branching ratios as well as the μ - e conversion rate in Titanium (green circles). Notice that whereas the current limit on $\text{BR}(\mu \rightarrow 3e)$ can be violated only at low masses, the one on $\text{CR}(\mu$ - e , Ti) can be exceeded over the entire viable range of dark matter masses. It is also important to stress that the rates of all these μ - e LFV processes do not extend to arbitrarily low values, and tend instead to lie up to few orders of magnitude below present bounds.

Figure 8 explores the correlations between the different μ - e LFV processes in this model. The left panel shows the viable points in the plane $\text{BR}(\mu \rightarrow e\gamma)$ vs. $\text{BR}(\mu \rightarrow 3e)$, whereas the right panel shows $\text{BR}(\mu \rightarrow e\gamma)$ vs. $\text{CR}(\mu$ - e , Ti). We also displayed, for each process, its current limit (solid lines) and its expected future sensitivity in planned experiments (dashed lines). As we have already observed in the previous figure, current limits on $\mu \rightarrow 3e$ and μ - e conversion in nuclei are not necessarily fulfilled and can be violated by more than two

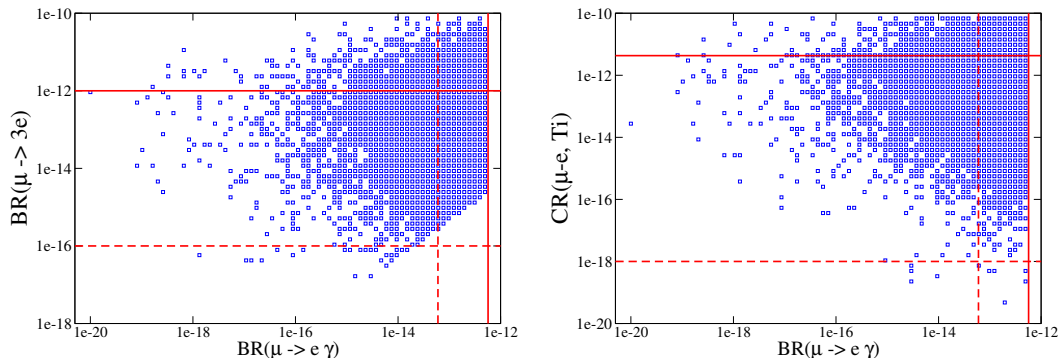


Figure 8: Left: The correlation between $\mu \rightarrow e\gamma$ and $\mu \rightarrow 3e$ for our sample of viable models. Right: The correlation between $\mu \rightarrow e\gamma$ and μ - e conversion in Titanium.

orders of magnitude. Thus, satisfying the $\mu \rightarrow e\gamma$ limit does not guarantee compatibility with other μ - e LFV experiments. In other words, contrary to the naive expectation, $\mu \rightarrow 3e$ and μ - e in nuclei may give a more stringent constraint than $\mu \rightarrow e\gamma$ for some models. Regarding future prospects, we see from the figure that the improvement in $\mu \rightarrow e\gamma$ though important will not be decisive as many models feature much smaller branching ratios. Completely different is the situation for $\mu \rightarrow 3e$ and μ - e in nuclei. There, the improvements will be more significant, and their impact will be crucial for this scenario. In fact, very few models lie beyond the expected sensitivity of future $\mu \rightarrow 3e$ or μ - e conversion experiments.

To emphasize this point, we plot instead $\text{BR}(\mu \rightarrow 3e)$ versus $\text{CR}(\mu$ - e , Ti) in Fig. 9. As noticed in the previous figure, only few points lie beyond the expected future sensitivity for either process. But now we can also observe that not a single point in our scan lies beyond the expected sensitivity for both processes. Future experiments searching for $\mu \rightarrow 3e$ and μ - e conversion in nuclei therefore have the potential to probe most, if not all, of the viable parameter space of this model.

5 Discussion

As we have seen, this model could be probed in future experiments via LFV processes. Other ways to test it include the direct [66] and indirect detection [67] of dark matter as well as searches at the LHC. In this section we give a brief look at these alternatives.

In our setup, the direct detection prospects are not very encouraging because the dark matter particle is leptophilic. Thus, it has a vanishing tree-level scattering cross section with nuclei. Radiative corrections will generate a non-zero cross section but it will still be highly suppressed. At one-loop, both the spin-independent interaction (mediated by the Higgs) and the anapole-moment (mediated by the photon) can be generated in this model. Recently, these one-loop effects were calculated explicitly within a similar radiative model [68] and it was found that the predicted signal lies well below the expected sensitiv-

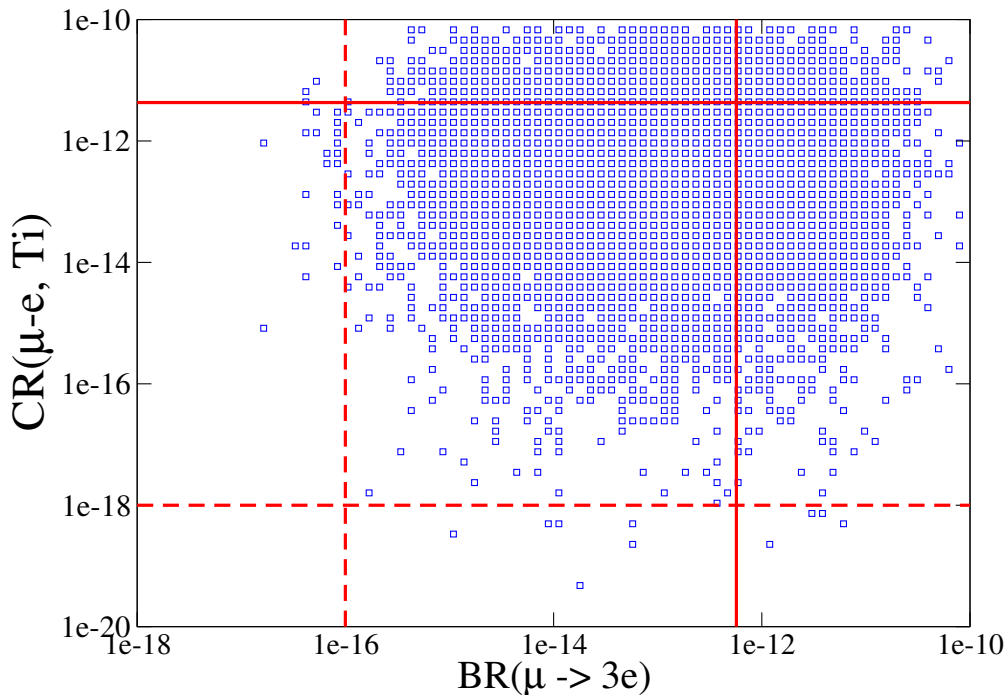


Figure 9: The correlation between $\mu \rightarrow 3e$ and μ - e conversion in nuclei for our sample of viable models.

ity of future experiments for the anapole-moment and just barely within it for the spin-independent one. In our scenario the situation is worse because the spin-independent cross section will be further suppressed by lepton masses or the $\beta_{1,2}$ parameters. We can safely conclude, therefore, that direct detection experiments cannot probe the viable parameter space of this model.

In spite of the velocity-suppressed annihilation cross section, the indirect detection of dark matter in this model is not entirely out of question. Notice that the velocity suppression in this setup is stronger than for Majorana fermions, featuring a v^4 rather than a v^2 behavior. Given that $v \sim 10^{-3}$ for dark matter particles in the galactic halo, this v^4 suppression implies an annihilation rate today about twelve orders of magnitude below the thermal one ($\sigma v \sim 3 \times 10^{-26} \text{ cm}^3 \text{ s}^{-1}$). This suppression can however be avoided with the emission of an additional photon, the so-called internal bremsstrahlung process [69], which gives rise to a gamma-ray feature at high energy. In [62, 70], where this effect was studied for scalar dark matter, it was found that, depending on the specific parameters of the model, this feature could actually be observed in current and planned gamma-ray telescopes. The other indirect detection channels – neutrinos, positrons and antiprotons – are not expected to play any role in constraining or testing this model.

As we have seen, our model predicts the existence of several particles with masses below the TeV scale. In particular, the charged fermion should have a mass below 600 GeV while the dark matter particle must be lighter than about 500 GeV. Naively, one would think that such particles should be easily produced

and detected at the LHC, but that is not really the case, as we now explain.

The LHC collaborations ATLAS and CMS have so far not performed any specific searches for models with radiative neutrino masses and dark matter candidates. Possible LHC constraints can therefore only be derived from analyses with leptonic signatures that are either model-independent or have been performed for models with similar additional physical states.

At first sight, our model bears some similarity with the Minimal Supersymmetric Standard Model (MSSM), where the heavy charged and neutral Z_2 -odd fermions are the charginos $\tilde{\chi}_1^\pm$ and the (often mass-degenerate) neutralinos $\tilde{\chi}_2^0$. However, contrary to the MSSM our fermions do not decay via cascades to a “golden” charged three-lepton final state, a neutrino and two light neutralinos $\tilde{\chi}_1^0$ carrying away missing transverse energy \cancel{E}_T , but directly to two charged leptons, a charged lepton and a neutrino or two neutrinos plus two invisible scalar dark matter particles. The trilepton ATLAS [71] and CMS [72] analyses do therefore not apply.

Two-lepton final states with \cancel{E}_T have also been analysed by ATLAS [73] and CMS [74], but under specific assumptions for the masses of the intermediate sleptons. While these assumptions are absent in the dilepton searches for Z' bosons [75, 76], the latter lack the \cancel{E}_T criterion. Single-lepton final states have been analysed in searches for W' bosons [77, 78] which rely, however, on the partial reconstruction of an s -channel resonance from the observed transverse mass not applicable here.

The ATLAS and CMS analyses cited above thus currently do not impose any direct limits on our model. The LHC data would have to be reanalysed with full signal, background and detector simulations. And even if we were to do so, which is beyond the scope of the present paper, the LHC data are not expected to significantly constrain the parameter space of this model.

6 Conclusions

We analyzed a TeV-scale extension of the SM that can simultaneously explain neutrino masses and the dark matter. The SM particle content was enlarged with a vector-like doublet of $SU(2)$, a singlet fermion, and two singlet scalars, all of them assumed to be odd under a Z_2 symmetry that guarantees the stability of the dark matter particle. In this scenario, neutrino masses are generated radiatively via one-loop processes mediated by the new fields. We examined the case where the dark matter particle – the lightest odd field – is a scalar and its relic density is determined by its Yukawa interactions. In this case, interesting correlations appear between dark matter, neutrino masses, and lepton flavor violating processes. We studied analytically and numerically the phenomenology of this scenario. We found that the dark matter constraint can only be satisfied for a dark matter mass below 500 GeV and a charged fermion mass below 600 GeV. We argued that neither existing collider searches at the LHC nor the dark matter direct or indirect detection searches can significantly constrain this scenario. A generic prediction of this setup is instead the existence of sizable rates for several LFV processes. In fact, they provide the most promising way of probing this model in the near future. Future searches for $\mu \rightarrow 3e$ and μ - e conversion in nuclei, in particular, have the potential to probe the entire parameter space of this model.

Acknowledgments

The work of M.K. and D.L. is supported by the BMBF under contract 05H15PMCCA and by the Helmholtz Alliance for Astroparticle physics. C.Y. is supported by the Max Planck Society in the project MANITOP.

References

- [1] G. Hinshaw et al. (WMAP), *Astrophys. J. Suppl.* **208**, 19 (2013), 1212.5226.
- [2] P. A. R. Ade et al. (Planck), *Astron. Astrophys.* **571**, A16 (2014), 1303.5076.
- [3] Y. Fukuda et al. (Super-Kamiokande Collaboration), *Phys.Rev.Lett.* **81**, 1562 (1998), [hep-ex/9807003](#).
- [4] Q. Ahmad et al. (SNO Collaboration), *Phys.Rev.Lett.* **89**, 011301 (2002), [nucl-ex/0204008](#).
- [5] T. Araki et al. (KamLAND Collaboration), *Phys.Rev.Lett.* **94**, 081801 (2005), [hep-ex/0406035](#).
- [6] D. V. Forero, M. Tortola, and J. W. F. Valle, *Phys. Rev.* **D90**, 093006 (2014), 1405.7540.
- [7] D. Restrepo, O. Zapata, and C. E. Yaguna, *JHEP* **11**, 011 (2013), 1308.3655.
- [8] S. Fraser, E. Ma, and O. Popov, *Phys. Lett.* **B737**, 280 (2014), 1408.4785.
- [9] D. Restrepo, A. Rivera, M. Sánchez-Peláez, O. Zapata, and W. Tangarife, *Phys. Rev.* **D92**, 013005 (2015), 1504.07892.
- [10] F. Bonnet, M. Hirsch, T. Ota, and W. Winter, *JHEP* **1207**, 153 (2012), 1204.5862.
- [11] K. A. Olive et al. (Particle Data Group), *Chin. Phys.* **C38**, 090001 (2014).
- [12] A. Zee, *Phys. Lett.* **B93**, 389 (1980), [Erratum: *Phys. Lett.*B95,461(1980)].
- [13] K. S. Babu, *Phys. Lett.* **B203**, 132 (1988).
- [14] L. M. Krauss, S. Nasri, and M. Trodden, *Phys. Rev.* **D67**, 085002 (2003), [hep-ph/0210389](#).
- [15] E. Ma, *Phys. Rev. Lett.* **81**, 1171 (1998), [hep-ph/9805219](#).
- [16] E. Ma, *Phys.Rev.* **D73**, 077301 (2006), [hep-ph/0601225](#).
- [17] Y. Farzan, *Phys. Rev.* **D80**, 073009 (2009), 0908.3729.
- [18] P. S. B. Dev and A. Pilaftsis, *Phys. Rev.* **D86**, 113001 (2012), 1209.4051.
- [19] Y. Farzan, S. Pascoli, and M. A. Schmidt, *JHEP* **03**, 107 (2013), 1208.2732.

- [20] S. S. C. Law and K. L. McDonald, JHEP **09**, 092 (2013), 1305.6467.
- [21] M. Hirsch, R. A. Lineros, S. Morisi, J. Palacio, N. Rojas, and J. W. F. Valle, JHEP **10**, 149 (2013), 1307.8134.
- [22] R. Longas, D. Portillo, D. Restrepo, and O. Zapata (2015), 1511.01873.
- [23] A. Vicente and C. E. Yaguna, JHEP **02**, 144 (2015), 1412.2545.
- [24] J. Casas and A. Ibarra, Nucl.Phys. **B618**, 171 (2001), hep-ph/0103065.
- [25] A. Ibarra and G. G. Ross, Phys.Lett. **B591**, 285 (2004), hep-ph/0312138.
- [26] W. Porod, F. Staub, and A. Vicente, Eur. Phys. J. **C74**, 2992 (2014), 1405.1434.
- [27] J. Adam et al. (MEG Collaboration), Phys.Rev.Lett. **110**, 201801 (2013), 1303.0754.
- [28] A. M. Baldini et al. (2013), 1301.7225.
- [29] B. Aubert et al. (BaBar Collaboration), Phys.Rev.Lett. **104**, 021802 (2010), 0908.2381.
- [30] T. Aushev et al. (2010), 1002.5012.
- [31] U. Bellgardt et al. (SINDRUM), Nucl. Phys. **B299**, 1 (1988).
- [32] A. Blondel et al. (2013), 1301.6113.
- [33] K. Hayasaka et al., Phys. Lett. **B687**, 139 (2010), 1001.3221.
- [34] C. Dohmen et al. (SINDRUM II), Phys. Lett. **B317**, 631 (1993).
- [35] T. P. working group (????).
- [36] A. Sato, PoS **NUFACT08**, 105 (2008).
- [37] W. H. Bertl et al. (SINDRUM II), Eur. Phys. J. **C47**, 337 (2006).
- [38] R. P. Litchfield, in *Interplay between Particle and Astroparticle physics London, United Kingdom, August 18-22, 2014* (2014), 1412.1406, URL <http://inspirehep.net/record/1332516/files/arXiv:1412.1406.pdf>.
- [39] H. Natori (DeeMe), Nucl. Phys. Proc. Suppl. **248-250**, 52 (2014).
- [40] S. Mihara, J. P. Miller, P. Paradisi, and G. Piredda, Ann. Rev. Nucl. Part. Sci. **63**, 531 (2013).
- [41] N. Arkani-Hamed, S. Dimopoulos, and S. Kachru (2005), hep-th/0501082.
- [42] R. Mahbubani and L. Senatore, Phys. Rev. **D73**, 043510 (2006), hep-ph/0510064.
- [43] F. D'Eramo, Phys. Rev. **D76**, 083522 (2007), 0705.4493.

- [44] R. Enberg, P. J. Fox, L. J. Hall, A. Y. Papaioannou, and M. Papucci, *JHEP* **11**, 014 (2007), 0706.0918.
- [45] T. Cohen, J. Kearney, A. Pierce, and D. Tucker-Smith, *Phys. Rev.* **D85**, 075003 (2012), 1109.2604.
- [46] C. Cheung and D. Sanford, *JCAP* **1402**, 011 (2014), 1311.5896.
- [47] L. Calibbi, A. Mariotti, and P. Tziveloglou, *JHEP* **10**, 116 (2015), 1505.03867.
- [48] C. E. Yaguna, *Phys. Rev.* **D92**, 115002 (2015), 1510.06151.
- [49] V. Silveira and A. Zee, *Phys. Lett.* **B161**, 136 (1985).
- [50] J. McDonald, *Phys. Rev.* **D50**, 3637 (1994), hep-ph/0702143.
- [51] C. Burgess, M. Pospelov, and T. ter Veldhuis, *Nucl.Phys.* **B619**, 709 (2001), hep-ph/0011335.
- [52] H. Davoudiasl, R. Kitano, T. Li, and H. Murayama, *Phys. Lett.* **B609**, 117 (2005), hep-ph/0405097.
- [53] V. Barger, P. Langacker, M. McCaskey, M. J. Ramsey-Musolf, and G. Shaughnessy, *Phys.Rev.* **D77**, 035005 (2008), 0706.4311.
- [54] R. Dick, R. B. Mann, and K. E. Wunderle, *Nucl. Phys.* **B805**, 207 (2008), 0803.1444.
- [55] C. E. Yaguna, *JCAP* **0903**, 003 (2009), 0810.4267.
- [56] A. Goudelis, Y. Mambrini, and C. Yaguna, *JCAP* **0912**, 008 (2009), 0909.2799.
- [57] S. Profumo, L. Ubaldi, and C. Wainwright, *Phys. Rev.* **D82**, 123514 (2010), 1009.5377.
- [58] C. E. Yaguna, *Phys. Rev.* **D81**, 075024 (2010), 1003.2730.
- [59] C. E. Yaguna, *JHEP* **1108**, 060 (2011), 1105.1654.
- [60] Y. Mambrini, *Phys. Rev.* **D84**, 115017 (2011), 1108.0671.
- [61] J. M. Cline, K. Kainulainen, P. Scott, and C. Weniger, *Phys. Rev.* **D88**, 055025 (2013), 1306.4710.
- [62] F. Giacchino, L. Lopez-Honorez, and M. H. G. Tytgat, *JCAP* **1310**, 025 (2013), 1307.6480.
- [63] P. Gondolo, J. Edsjo, P. Ullio, L. Bergstrom, M. Schelke, and E. A. Baltz, *JCAP* **0407**, 008 (2004), astro-ph/0406204.
- [64] G. Belanger, F. Boudjema, A. Pukhov, and A. Semenov, *Comput. Phys. Commun.* **185**, 960 (2014), 1305.0237.
- [65] F. Staub, T. Ohl, W. Porod, and C. Speckner, *Comput. Phys. Commun.* **183**, 2165 (2012), 1109.5147.

- [66] P. Cushman et al., in *Community Summer Study 2013: Snowmass on the Mississippi (CSS2013) Minneapolis, MN, USA, July 29-August 6, 2013* (2013), 1310.8327, URL <http://inspirehep.net/record/1262767/files/arXiv:1310.8327.pdf>.
- [67] J. Buckley et al., in *Community Summer Study 2013: Snowmass on the Mississippi (CSS2013) Minneapolis, MN, USA, July 29-August 6, 2013* (2013), 1310.7040, URL <http://inspirehep.net/record/1262275/files/arXiv:1310.7040.pdf>.
- [68] A. Ibarra, C. E. Yaguna, and O. Zapata, *Phys. Rev.* **D93**, 035012 (2016), 1601.01163.
- [69] T. Bringmann, L. Bergstrom, and J. Edsjo, *JHEP* **01**, 049 (2008), 0710.3169.
- [70] T. Toma, *Phys. Rev. Lett.* **111**, 091301 (2013), 1307.6181.
- [71] G. Aad et al. (ATLAS) (2015), 1509.07152.
- [72] V. Khachatryan et al. (CMS Collaboration) (2014), 1405.7570.
- [73] G. Aad et al. (ATLAS Collaboration), *JHEP* **1405**, 071 (2014), 1403.5294.
- [74] C. Collaboration (CMS) (2013).
- [75] T. A. collaboration (2015).
- [76] C. Collaboration (CMS) (2015).
- [77] ATLAS Collaboration (2015).
- [78] CMS Collaboration (CMS) (2015).